Electrical Power and Energy Systems 58 (2014) 75–84

Contents lists available at ScienceDirect

Electrical Power and Energy Systems

journal homepage: www.elsevier.com/locate/ijepes

Input–output signal selection for damping of power system oscillations using wind power plants

José Luis Domínguez-García [a,*], Carlos E. Ugalde-Loo [c], Fernando Bianchi [a], Oriol Gomis-Bellmunt [a,b]

[a] IREC Catalonia Institute for Energy Research, Jardins de les Dones de Negre 1, 2a, Sant Adrià de Besòs, 08930 Barcelona, Spain
[b] Centre d'Innovació Tecnològica en Convertidors Estàtics i Accionaments (CITCEA-UPC), Universitat Politècnica de Catalunya UPC, Av. Diagonal, 647, Pl. 2, 08028 Barcelona, Spain
[c] Institute of Energy, Cardiff University, Queen's Buildings, The Parade, CF24 3AA Cardiff, Wales, UK

ARTICLE INFO

Article history:
Received 4 April 2013
Received in revised form 10 December 2013
Accepted 1 January 2014

Keywords:
Controllability
Damping
Frequency domain analysis
Observability
Power system oscillation
Wind power plant

ABSTRACT

During the last years wind power has emerged as one of the most important sources in the power generation share. Due to stringent Grid Code requirements, wind power plants (WPPs) should provide ancillary services such as fault ride-through and damping of power system oscillations to resemble conventional generation. Through an adequate selection of input–output signal pairs, WPPs can be effectively used to provide electromechanical oscillations damping. In this paper, different analysis techniques considering both controllability and observability measures and input–output interactions are compared and critically examined. Recommendations are drawn to select the best signal pairs available from WPPs to contribute to power oscillations damping. Control system design approaches including single-input single-output and multivariable control are considered. The recommendation of analysis techniques is justified through the tools usage in a test system including a WPP.

1. Introduction

As a consequence of increased wind power penetration levels, transmission system operators (TSOs) are concerned with system stability. Wind power plants (WPPs) are required by TSOs to meet Grid Code requirements and sometimes to behave as conventional power plants — capable of providing support to the power system when requested to maintain stability [1–3]. Power system stability is divided in three main groups depending on the response of the system to a fault: frequency, rotor angle and voltage stability [4].

Rotor angle stability is defined as the capability of synchronous generators to keep or restore the equilibrium between their mechanical and electromagnetic torques. This stability issue is usually exhibited by synchronous generators as low frequency oscillations (LFOs). The main effects of such oscillations are to limit the power transfer capacity of the system and to cause large grid failures. This problem used to be solved by the installation of power system stabilizers (PSSs) at synchronous generators to increase the damping of the system. Nowadays, due to recent technological advances on power system devices, damping of electromechanical oscillations has been proposed in the literature to be provided by HVDC links, energy storage systems, flexible AC transmission systems and wind power generation [5–10]. It is worth mentioning that wind power is located where wind blows stronger and is more profitable; thus, it is difficult to geographically locate a WPP where its damping capabilities can be best achieved [11]. The physical location of the WPP plays an important role when defining the possible input and output signals for oscillation mitigation if they are measured locally [7,11]. When the WPP is far from the conventional generation, the low frequency oscillation on the electrical signals can be smoothed or hidden. This implies a lower observability, as stated in [7,11].

Different methods to select the best feedback signal to damp power oscillations have been discussed in [8,12–16], but the case for WPPs has not been yet well covered. Recent research focuses on the best input–output signal pairs employing controllability and observability analyses such as residues and geometric measures [13,17]. Other works study the interaction between different controllers for a multiple-input multiple-output (MIMO, multivariable) case and try to determine if a decentralized controller could be considered by using the relative gain array (RGA) [17,18]. In [19], fundamental limitations of control design by using local signals to damp remote oscillations are analyzed, where the interaction between local and remote signals has an important influence.

The aim of this paper is to compare different controllability and observability and signal interaction analyses for power system oscillation damping employing local signals from WPPs. The main

* Corresponding author. Tel.: +34 933562615; fax: +34 933563802.
E-mail address: jldominguez@irec.cat (J.L. Domínguez-García).

0142-0615
http://dx.doi.org/10.1016/j.ijepes.2014.01.001

advantages and drawbacks of each alternative are examined. Frequency domain tools such as the RGA and the multivariable structure function (MSF) [20–22] are employed to assess the interaction between signal pairs. Using the frequency domain approach, the arising control design and performance limitations under the presence of right hand plane zeros (RHPZs) are clearly defined [23]. The use of some of these methods is recommended to select the best input–output pairs which ensure a good controllability and observability of the desired oscillation mode, while providing a clear insight of the potential and limitations of the damping controller. These suggestions provide a guideline to select the best input–output signal pairs suitable to damp power system oscillations by means of WPPs signals –either through single-input single-output (SISO) or multivariable (MIMO) control schemes.

2. Contribution of WPPs to damp power system oscillations

WPPs comprising variable-speed wind turbines only (either based on doubly-fed induction generators or fully-rated converters) exhibit dynamics which are considerably faster than the synchronous frequency and the electromechanical dynamics found within power systems. Decoupling of WPPs from network dynamics can be achieved through the use of power converters [3]. For these reasons, WPP models can be simplified for small-signal stability analysis.

WPPs regulate the active power delivered to the grid through an adequate control of the generator-side converter. The aim is to transfer the maximum active power from the wind turbine following an optimum wind power extraction. On the other hand, reactive power regulation is achieved through the control of the grid-side converter [24]. Due to the availability of active and reactive power measurements for converter control, these could be used potentially as control signals for damping controllers. In general, either local or remote measurements could be selected as input signals for a damping controller sitting at a WPP, where electrical variables can be represented, for convenience, as phasors (*i.e.*, in terms of their magnitude and phase angle).

It should be emphasized that the input–output pair (or pairs) selection largely influences the performance of power oscillation dampers. This is particularly critical for the case of WPPs, since they can be located far away from the synchronous generators — where electromechanical oscillations originate.

In general, power systems can be described by a set of nonlinear differential and algebraic equations of the form

$$\begin{aligned} \dot{x} &= f(x,u) \\ y &= l(x,u) \end{aligned} \tag{1}$$

where $x = [x_1, x_2, \ldots, x_n]^T$ is the state, $u = [u_1, u_2, \ldots, u_m]^T$ is the input, $y = [y_1, y_2, \ldots, y_r]^T$ is the output, and $f(\cdot) = [f_1(\cdot), f_2(\cdot), \ldots, f_n(\cdot)]^T$ and $l(\cdot) = [l_1(\cdot), l_2(\cdot), \ldots, l_n(\cdot)]^T$ are nonlinear functions [4].

For small signal analysis, system (1) is linearized around an operating point and can be written in state-space form as

$$\begin{aligned} \Delta\dot{x} &= A\Delta x + B\Delta u \\ \Delta y &= C\Delta x + D\Delta u \end{aligned} \tag{2}$$

where Δx, Δu and Δy are small deviations with respect to the operating point (thereinafter, the Δ symbol is omitted for simplicity); A, B, C, and D are matrices of adequate dimensions; and the corresponding transfer function is given by

$$G(s) = C(sI - A)^{-1}C + D. \tag{3}$$

Fig. 1 shows a feedback loop using a controller K relating the inputs with the outputs of system. It is worth to remark that K represents any linear time-invariant controller.

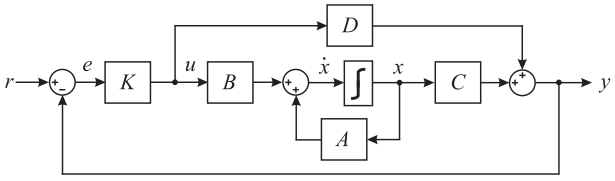

Fig. 1. Block diagram of a plant with feedback.

If power oscillation damping is provided by WPPs, the system inputs (or control signals) could be the active (P_{wt}) and the reactive power (Q_{wt}) delivered by the WPP. Conversely, the outputs (or measured signals) could be defined as the voltage magnitude (V_{wt}) and the voltage phase angle (θ_{wt}) at the point of connection of the WPP. The availability of these signal measurements provides different control alternatives, including both SISO and MIMO control schemes. For instance, if a SISO controller is considered, the input–output pair could be chosen, for example, as $u = P_{wt}$ with $y = V_{wt}$, or alternatively $u = Q_{wt}$ with $y = V_{wt}$, among others.

For the MIMO case, both inputs and outputs should be considered at the same time (*i.e.*, $u = [P_{wt} Q_{wt}]^T$, $y = [V_{wt} \theta_{wt}]^T$). The control scheme could be either centralized or decentralized. In the case of a decentralized controller, the input–output signal pair definition arising from a diagonal control structure has significant importance when designing effective controllers [23]. The pairing selection criteria for both SISO and MIMO control schemes are commonly based on controllability and observability properties, and performance limitations are established following a frequency response analysis of the open loop system [25,26].

3. Input–output selection methods

3.1. Controllability and observability measures

Controllability indicates how the state variables describing the behavior of a system can be affected by its inputs. Observability is associated with the possibility of determining the states from the outputs. More precisely, the system (2) is said to be controllable, if for any initial state $x(t_0)$, $t_1 > 0$ and final state x_1, there exists finite input u such that $x(t_1) = x_1$. The system (2) is observable if, for any $t_1 > 0$, the initial state $x(t_0)$ can be determined from $u(t_1)$ and $y(t_1)$ [23].

In damping of power oscillations, it is necessary to determine controllability and observability for specific eigenvalues. A brief description of tools commonly used for this purpose is presented next.

3.1.1. Popov–Belevitch–Hautus (PBH) test

This consists in evaluating the rank of matrices

$$\mathcal{C}(\lambda_k) = [\,\lambda_k I - A \quad b_i\,] \tag{4}$$

$$\mathcal{O}(\lambda_k) = [\,\lambda_k I - A \quad c_j\,]^T \tag{5}$$

where λ_k is the kth eigenvalue of the matrix A, I is the identity matrix, b_i is the column of B corresponding to ith input u_i and c_j is the row of C corresponding to the jth output y_j. The mode λ_k of linear system (2) is controllable if matrix $\mathcal{C}(\lambda_k)$ has full row rank. Similarly, the mode λ_k is observable if $\mathcal{O}(\lambda_k)$ is full column rank [23].

The rank of matrices $\mathcal{C}(\lambda_k)$ and $\mathcal{O}(\lambda_k)$ can be evaluated by their singular values. The singular values of a matrix M are defined as $\sigma_i = \sqrt{\lambda_k(M^T M)}$ $(k = 1, \ldots, n)$ with $\sigma_1 \geqslant \ldots \geqslant \sigma_n \geqslant 0$. The matrix rank is then given by the number of non-null singular values. In practice, due to numerical limitations, the rank is the number of singular values greater than a given tolerance. Therefore, the minimum singular values σ_n provide a measure of how close to

singular is the matrix. In the case of matrices $\mathcal{C}(\lambda_k)$ and $\mathcal{O}(\lambda_k)$, σ_n indicates how far is the system of being uncontrollable or unobservable, respectively, with respect to the ith input and jth output.

The choice of input and output signals through the PBH test is done by selecting those with the largest of the minimum singular values σ_n of matrices $\mathcal{C}(\lambda_k)$ and $\mathcal{O}(\lambda_k)$ [12]. Although this is a reasonable input–output selection criterion to determine the most controllable and observable signals, it is not always clear which pair presents the best joint controllability and observability characteristics. From a control point of view, the joint measure is of great importance.

3.1.2. Residue analysis

Given the transfer function $g_{ij}(s)$ from the input u_i to the output y_j, it is always possible to express it as a sum of partial fractions of the form

$$g_{ij}(s) = \frac{y_j(s)}{u_i(s)} = c_j(sI - A)^{-1}b_i + d_{ij} = \sum_{k=1}^{n} \frac{R_k}{s - \lambda_k} + d_{ij} \tag{6}$$

where R_k is the residue associated to the mode λ_k [26]. The residue R_k provides an idea of how the mode λ_k is affected by the input u_i and how visible is from the output y_j. Therefore, the residues are clear measures of joint controllability and observability of a particular oscillation mode. For this reason, residues are commonly used in damping oscillation analysis [4,13,27].

The residues can be computed directly from the state-space realization by using

$$R_k = c_j\phi_k\psi_k b_i \tag{7}$$

where ϕ_k and ψ_k are the right and left eigenvectors of the matrix A, respectively, corresponding to the eigenvalue λ_k. As in general the residues are complex numbers, the best input–output signal pair is given by the maximum value of the residue magnitude. The residues depend on the scale of the input and output signals and do not always provide a clear comparison among transfer functions associated to variables with different units.

3.1.3. Geometric measures

The controllability and observability geometric measures, respectively, are defined as

$$m_{ci} = \cos(\theta(\psi_k, b_i)) = \frac{|b_i^T\psi_k|}{\|\psi_k\|\|b_i\|} \tag{8}$$

$$m_{oj} = \cos(\theta(\phi_k, c_j)) = \frac{|c_j\phi_k|}{\|\phi_k\|\|c_j\|} \tag{9}$$

where $\theta(\psi_k, b_i)$ is the angle between b_i and ψ_k, and $\theta(\phi_k, c_j)$ is the angle between c_j and ϕ_k. The geometric measures provide an idea of how aligned the columns of matrix B and the rows of C are with an eigenvector of A. If $m_{ci} = 0$, the column of b_i is orthogonal to eigenvector ψ_k and a controller will not be effective to modify the state associated to eigenvalue λ_k. Similarly, if $m_{oj} = 0$, c_j and ϕ_k are orthogonal and mode λ_k will not be observable from the output y_j [28].

A joint geometric measure can be defined as

$$m_{coij} = m_{ci}m_{oj}. \tag{10}$$

A zero value of m_{coij} indicates that λ_k is non-controllable/non-observable from the ith input and the jth output. The geometric measures provide a similar information as the residues, with the advantage of being normalized and independent of the scale of the signals. These measures have been used to determine the best input–output pair in power oscillation damping applications [14,28].

Some authors have proposed the use of Hankel singular values (HSVs) for the selection of input–output pairs [8]. However, it is not possible to connect the controllability and observability of a particular mode with the HSVs [23]. For this reason, their use is not considered in this paper.

3.2. Limitations caused by RHPZs

It is well-known that non-minimum phase zeros (or RHPZ) impose limitations on the achievable performance [29,30]. To ensure closed-loop stability, the controller cannot cancel RHPZs and the frequency response of the closed-loop transfers will have fixed points that cannot be altered by the controller. For instance, the sensitivity transfer $S(s)$ takes the value 1 at a RHPZ independently of the controller; that is, if ξ is a RHPZ, then

$$S(\xi) = (I + K(\xi)G(\xi))^{-1} = 1. \tag{11}$$

These constraints become serious limitations if the RHPZs are close to the mode to be damped, since the magnitude of the closed-loop transfer cannot be arbitrarily reduced. If the controller set is reduced to proportional gains, the constraints are more serious. A simple root locus analysis reveals how strong these limitations are. Since the closed-loop poles tend to the open loop zeros, if an open loop pole is close to a RHPZ, a small increment in gain may result in an unstable system and thus it is not possible to affect the lightly damped mode. Therefore, any pair with RHPZs in the range of LFOs should be avoided.

The limitations imposed by RHPZs have been used to propose input–output selection procedures in [30,31]. In the context of damping oscillations in power systems they have been used in [8,19].

3.3. Input–output interactions

An alternative view on input–output signal pair selection can be obtained from the frequency domain. This allows to evaluate input–output interactions and thus determine if decentralized controllers will be able to achieve a reasonable closed-loop behavior.

3.3.1. RGA

It allows to evaluate interactions among different inputs and outputs [23]. In the context of input–output pair selection, it helps to determine the pair with the highest interaction and to evaluate the possibility of using multivariable controllers. The RGA matrix H is defined as

$$H(s) = [\eta_{ij}(s)] = G(s) \otimes G(s)^{-T} \tag{12}$$

where $[\eta_{ij}]$ denotes the element ij of the matrix H and the operator $\otimes$ denotes the Hadamard or Schur product (element by element product) [23].

For example, in case of systems with two inputs and two outputs (2×2 system),

$$G(s) = \begin{bmatrix} g_{11}(s) & g_{12}(s) \\ g_{21}(s) & g_{22}(s) \end{bmatrix} \tag{13}$$

and the RGA is given by

$$H(s) = \begin{bmatrix} \eta_{11}(s) & 1 - \eta_{11}(s) \\ 1 - \eta_{11}(s) & \eta_{11}(s) \end{bmatrix} \tag{14}$$

with

$$\eta_{11}(s) = \frac{g_{11}(s)g_{22}(s)}{g_{11}(s)g_{22}(s) - g_{12}(s)g_{21}(s)}. \tag{15}$$

The following conclusions can be drawn from the RGA (14) [20,23]:

- If η_{11} is close to 1, pairs $u_1 - y_1$ and $u_2 - y_2$ are decoupled and can be controlled independently. In this case, a centralized multivariable controller will not achieve a better performance than the decentralized one

$$K(s) = \begin{bmatrix} k_{11}(s) & 0 \\ 0 & k_{22}(s) \end{bmatrix}, \tag{16}$$

in which k_{11} and k_{22} can be designed independently.
- If η_{11} is close to zero, the RGA indicates that the best pairs for decentralized control should be $u_1 - y_2$ and $u_1 - y_2$ and the controllers can be designed independently if the input–output pairs are reordered.
- Otherwise, the pairs are not decoupled and the decentralized controller should be designed carefully. For stable plants, input–output pairs with negative steady-state RGA elements should be avoided. Otherwise, if the sub-controllers are designed independently each with integral action, then the interactions will cause instability either when all the loops are closed or when the loop corresponding to the negative relative gain becomes inactive.

Notice that the RGA depends on the frequency. Therefore, the previous analysis should be done in the frequency range of interest; *i.e.*, the range where LFOs arise.

3.3.2. MSF

It is the building block for the individual channel analysis and design (ICAD) framework [32,33]. An appropriate interpretation of the MSF at low and high frequency allows to determine: the existence and required structure of diagonal controllers, the dynamical structure of the closed-loop system, a reliable measurement of robustness, and the possibility to satisfy design specifications [20].

In ICAD, the dynamical structure of $G(s)$ is determined by individual channels $C_i(s)$ resulting from pairing each input to each output by means of diagonal controllers [32]. Consider the 2×2 system in (13) and the decentralized controller (16). Then the closed-loop system can be represented as two SISO individual channels $C_i(s)$, each including a feedback loop and its controller, as shown in Fig. 2. The multivariable structure of the plant is encapsulated by the scalar transfer function $\gamma_a(s)$. This representation is equivalent to the original system with no loss of information [32].

In general, $C_i(s)$ has the open loop SISO transmittance

$$C_i(s) = k_{ii}(s)g_{ii}(s)(1 - \gamma_a(s)h_j(s)) \tag{17}$$

where

$$\gamma_a(s) = \frac{g_{12}(s)g_{21}(s)}{g_{11}(s)g_{22}(s)} \tag{18}$$

is the MSF and

$$h_j(s) = \frac{k_{jj}(s)g_{jj}(s)}{1 + k_{jj}(s)g_{jj}(s)} \tag{19}$$

describes the impact of controller $k_{jj}(s)$ on the ith control loop, subjected to the disturbances

$$d_i = \frac{g_{ij}(s)}{g_{jj}(s)}h_j(s)r_j(s), \tag{20}$$

which represent the effect of reference $r_j(s)$ on channel $C_i(s)$. As it can be seen from Fig. 2 and (17)–(20) the behavior of $C_i(s)$ is both affected by its controller $k_{ii}(s)$ and by channel $C_j(s)$ [32,33]. Moreover, the MSF [20]:

- determines the dynamical characteristics of each input–output configurations and indicates the potential performance of a feedback control system;
- its adequate interpretation ensures an effective control system design;
- its magnitude quantifies the coupling between input–output channels in the frequency domain,
- is related to the plant transmission zeros (zeros of $1 - \gamma_a(s), |G(s)| = g_{11}(s)g_{22}(s) - g_{12}(s)g_{21}(s) = 0$);
- $\gamma_a(s) = 1$ determines the non-minimum phase condition;
- its closeness to (1,0) in the Nyquist plot indicates to what extent the plant is sensitive to uncertainty in terms of gain and phase margins.

If the channels are defined by pair $u_1 - y_2$ and $u_2 - y_1$, then the MSF is given by

$$\gamma_b(s) = \frac{g_{11}(s) \cdot g_{22}(s)}{g_{12}(s) \cdot g_{21}(s)} = \gamma_a^{-1}(s) \tag{21}$$

and

$$C_i(s) = k_{ij}(s)g_{ji}(s)(1 - \gamma_b(s)h_j(s)). \tag{22}$$

Notice that the RGA matrix H can be expressed in terms of the MSFs [20]:

$$H = \begin{bmatrix} \frac{1}{1-\gamma_a(s)} & \frac{\gamma_a(s)}{\gamma_a(s)-1} \\ \frac{\gamma_a(s)}{\gamma_a(s)-1} & \frac{1}{1-\gamma_a(s)} \end{bmatrix} = \begin{bmatrix} \frac{\gamma_b(s)}{\gamma_b(s)-1} & \frac{1}{1-\gamma_b(s)} \\ \frac{1}{1-\gamma_b(s)} & \frac{\gamma_b(s)}{\gamma_b(s)-1} \end{bmatrix}. \tag{23}$$

4. Case study

The different methods presented in Section 3 are assessed through the test system shown in Fig. 3, which has been previously used to show the interaction between conventional generation and WPPs [34]. This is a simple power system model which provides a clear insight of the system dynamics. The WPP including converter-based wind turbines is assumed as a negative load, since the converter dynamics are considerably faster than the electromechanical dynamics that this work is focused on. For the same rea-

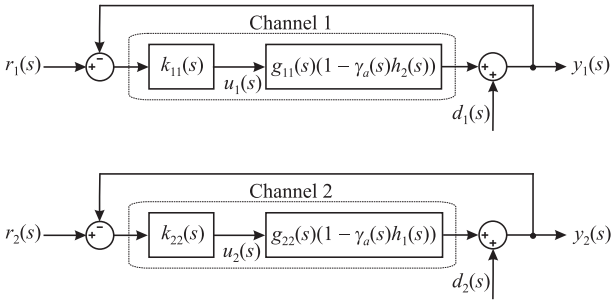

Fig. 2. Individual channel representation of a 2 × 2 system.

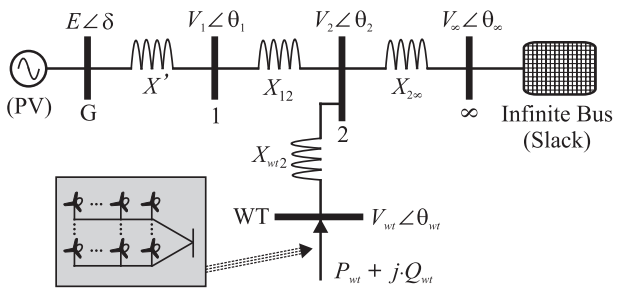

Fig. 3. Electrical network representation of the power system under study.

son, the transmission lines are modeled as reactances, with the capacitor dynamics in PI representations being neglected. This approach has been previously used in [35]. The system parameters can be found in Appendix A.

The linearized system is represented in state-space form as (2), where

$$x = [\delta \omega E']^T, \quad u = [P_{wt} Q_{wt}]^T, \quad y = [V_{wt} \theta_{wt}]^T \tag{24}$$

The state variables x represent the angle and frequency of the rotor and the exciter control variable of the synchronous machine. The input u is the aggregated active and reactive power and the output y is the voltage magnitude and phase angle of the WPP. Matrix A has a lightly damped oscillation mode at $\lambda_{12} = -0.0119 \pm 8.30375j$, with frequency 1.322 Hz and a damping coefficient of 0.00144.

As it can be seen from (24), the system is 2×2. Although simple in nature, it is representative enough to clearly assess the tools presented in Section 3. The use of a more complex system representation is out of the scope of this work; however, the tools here presented could be equally applied to systems with additional inputs and outputs. It should also be noted that the impact of measuring remote signals using wide-area measurement systems could be included through the introduction of time delays, but it is out of scope of this paper. Instead, it is assumed that all signals are available (either through direct measurement or estimation).

4.1. Controllability and observability measures comparison

The controllability and observability measures previously presented were compared using the system under study. According to (24), four possible signal pairs can be analyzed: $P_{wt} - V_{wt}$, $Q_{wt} - V_{wt}$, $P_{wt} - \theta_{wt}$ and $Q_{wt} - \theta_{wt}$.

4.1.1. PBH test

The singular values corresponding to $\mathcal{C}(\lambda_1)$ and $\mathcal{O}(\lambda_1)$ are listed in Tables 1 and 2. Notice that matrix $\mathcal{C}(\lambda_1)$ depends on vectors b_i and not on c_j. For this reason, Table 1 has only two columns. The same applies to $\mathcal{O}(\lambda_1)$, with results in Table 2. The largest of the minimum singular values for the possible signal pairs is highlighted. It can be observed that the most controllable pairs correspond to those with the active power delivered by the WPP (P_{wt}) as an input. The most observable pairs are those with the phase angle of the WPP connection point (θ_{wt}) as an output.

It can be concluded that the best signal pair is $P_{wt} - \theta_{wt}$ since it renders the largest of the minimum singular values for both $\mathcal{C}(\lambda_1)$ and $\mathcal{O}(\lambda_1)$. Also, it can be seen that the worst signal pair is $Q_{wt} - V_{wt}$. However, the next best possible option is not clear from the remaining alternatives since the PBH test does not provide any joint controllability and observability measure.

Table 1
Singular values of matrix $\mathcal{C}(\lambda_1)$.

$P_{wt} - V_{wt}/P_{wt} - \theta_{wt}$	$Q_{wt} - V_{wt}/Q_{wt} - \theta_{wt}$
78.9950	77.6115
8.3223	8.3224
1.6480	0.5251

Table 2
Singular values of matrix $\mathcal{O}(\lambda_1)$.

$P_{wt} - V_{wt}/Q_{wt} - V_{wt}$	$P_{wt} - \theta_{wt}/Q_{wt} - \theta_{wt}$
77.461	77.462
8.329	8.323
0.002	**0.045**

Table 3
Residue values.

	$P_{wt} - V_{wt}$	$Q_{wt} - V_{wt}$	$P_{wt} - \theta_{wt}$	$Q_{wt} - \theta_{wt}$
$\lvert R_i \rvert$	0.018	0.006	**0.349**	0.109

4.1.2. Residue analysis

The magnitudes of the residues are listed in Table 3. It can be observed that the maximum value corresponds to the pair $P_{wt} - \theta_{wt}$. This is consistent with the information provided by the PBH test; thus, this signal pair should be selected as a first option. Conversely to the PBH test, the residue analysis clearly defines the best order of the signal pairs due to its joint controllability and observability measurement test.

4.1.3. Geometric measures

These are given in Table 4. The joint controllability and observability measure m_{co} shows that the signal pair to be selected must be $P_{wt} - \theta_{wt}$ since it has the maximum value among the input–output pairs. This pair presents negligible differences compared to $Q_{wt} - \theta_{wt}$ in terms of controllability and observability; in other words, the use of either pair would provide similar results. These results are consistent with those obtained previously. However, in this case the information is clearer since the values are normalized and presented in per unit.

4.2. RPHZs

The transfer function corresponding to the system under analysis is given by $G(s)$ in (13), where

$$\begin{aligned}
g_{11}(s) &= -\frac{0.032727(s+0.5314)(s^2-0.08487s+78.87)}{(s+0.3985)(s^2+0.02391s+68.95)} \\
g_{12}(s) &= \frac{0.23117(s+0.4832)(s^2+0.01688s+69.35)}{(s+0.3985)(s^2+0.02391s+68.95)} \\
g_{21}(s) &= \frac{0.23766(s+0.4036)(s^2+0.0181s+93.34)}{(s+0.3985)(s^2+0.02391s+68.95)} \\
g_{22}(s) &= -\frac{0.021838(s+0.535)(s^2-0.2433s+151.9)}{(s+0.3985)(s^2+0.02391s+68.95)}
\end{aligned} \tag{25}$$

Fig. 4 shows the Bode plots of the individual transfer functions in (25). For clarity, Fig. 4(a) features the diagonal elements $g_{ii}(s)$ and Fig. 4(b) the off-diagonal entries $g_{ij}(s)$ of $G(s)$. It can be clearly seen that the damping controller should act in the region 8–11 rad/s (1.2–1.75 Hz).

In Eq. (25), it can be seen a pair of complex RHPZs in the individual transfer functions $g_{11}(s)$ and $g_{22}(s)$ close to the lightly damped mode $\lambda_{12} = -0.01196 \pm j8.3038$. In the Bode plots in Fig. 4(a), a resonance peak caused by the low damping of λ_{12} can be observed. The contribution of 180 degrees of the non-minimum phase zeros is also clear in these plots. In the rest of the frequencies, the magnitudes of $g_{11}(s)$ and $g_{22}(s)$ are below −20 dB, suggesting a small contribution of input P_{wt} to output V_{wt} and input Q_{wt} to output θ_{wt}. Fig. 4(b) shows $g_{12}(s)$ and $g_{21}(s)$. The proximity of the oscillation mode λ_{12} to the lightly damped zeros tends to cancel the resonances peaks; however, in these cases the minimum phase

Table 4
Geometric measures.

	$P_{wt} - V_{wt}$	$Q_{wt} - V_{wt}$	$P_{wt} - \theta_{wt}$	$Q_{wt} - \theta_{wt}$
m_c	**0.9928**	0.9927	**0.9928**	0.9927
m_o	0.3842	0.3842	**0.9505**	**0.9505**
m_{co}	0.3815	0.3814	**0.9437**	0.9436

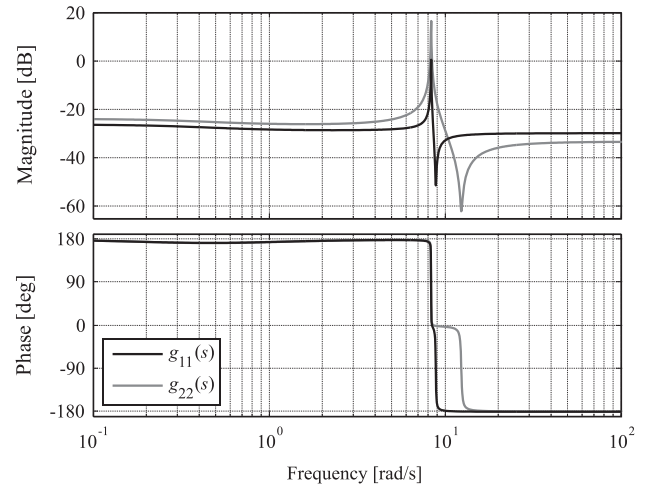

(a) $g_{11}(s)$ and $g_{22}(s)$

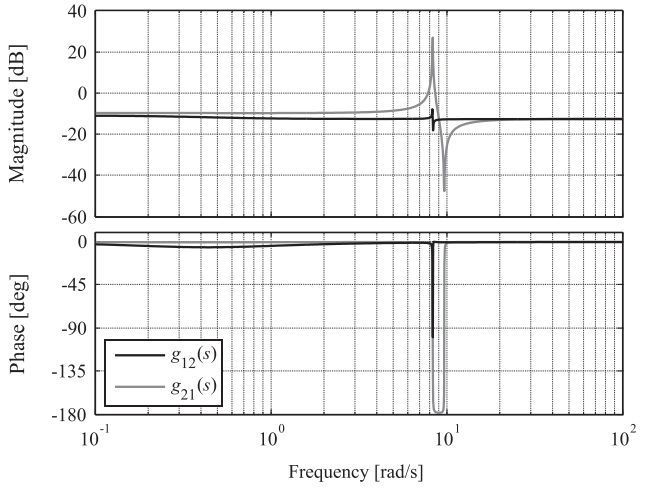

(b) $g_{12}(s)$ and $g_{21}(s)$

Fig. 4. Bode diagrams of transfer functions $g_{ij}(s)$.

zeros contribute with positive phase. The magnitude of transfer functions $g_{ij}(s)$ is higher compared to that of $g_{ii}(s)$.

If disturbances at the voltage are considered, the closed-loop transfer is given by

$$g_{cl,ij}(s) = (1 + K_{ij}(s)g_{ij}(s))^{-1}. \tag{26}$$

Due to the RHPZs in g_{11} and g_{22} ($\xi_{11} = 0.0424 \pm 8.8808j$ and $\xi_{22} = 0.1216 \pm 12.3242j$), regardless the controller

$$g_{cl,11}(\xi_{11}) = g_{cl,22}(\xi_{22}) = 1. \tag{27}$$

This implies that it will be difficult to reduce the resonance peak and thus to increase the damping of mode λ_{12}, especially in case of g_{11} where ξ_{11} is quite close to λ_{12} [29].

This preliminary analysis suggests avoiding signal pairs directly associated to individual elements $g_{11}(s)$ and $g_{22}(s)$ due to the limitations imposed by the presence of RHPZs; *i.e.*, avoid $P_{wt} - V_{wt}$ and $Q_{wt} - \theta_{wt}$. Nevertheless, since no conclusion has been made about the internal coupling of the plant it is not apparent how the RHPZs of $g_{11}(s)$ and $g_{22}(s)$ will reflect on the signal pairs associated to off-diagonal transfer functions $g_{12}(s)$ and $g_{21}(s)$ (*i.e.*, on pairs $P_{wt} - \theta_{wt}$ and $Q_{wt} - V_{wt}$).

4.3. Input–output interactions

The methods previously presented for determining suitable input–output pairs are used to analyze the system under study (Fig. 3).

4.3.1. RGA

The elements of matrix H for the 2×2 system are

$$\eta_{11} = \frac{-0.0132(s+0.54)(s+0.53)(s^2-0.085s+77.87)(s^2-0.24s+154.9)}{(s+0.484)(s+0.398)(s^2+0.0239s+68.95)(s^2+0.018s+92.85)}$$
$$\eta_{12} = \frac{1.013(s+0.48)(s+0.4)(s^2+0.017s+69.35)(s^2+0.018s+93.34)}{(s+0.484)(s+0.398)(s^2+0.0239s+68.95)(s^2+0.018s+92.85)} \tag{28}$$

Fig. 5 shows the Bode diagrams of the diagonal and off-diagonal RGA entries. It can be seen that $\eta_{11}(s)$ (diagonal elements of H) are negative for most frequencies and their magnitude small. This can be concluded after examination of (28) and the phase plot in Fig. 5. Phases of 180° and −540° correspond to negative magnitudes, and overall $\eta_{11}(s)$ will only be positive for a narrow margin of frequencies between 8 and 10 rad/s. Conversely, the magnitude of $\eta_{12}(s)$ (off-diagonal elements of H) is close to unity (*i.e.*, 0 dB), as shown by Fig. 5. Simple inspection of (28) shows that $\eta_{12}(s)$ has a positive magnitude for all frequencies. This is corroborated by the nearly constant phase of 0° in Fig. 5.

As outlined in Section 3.3, in case of using decentralized controllers with independently designed elements, input–output pairs with positive diagonal (or off-diagonal) entries are recommended. Since the magnitude of $\eta_{11}(s)$ is negative for most frequencies, pairs $P_{wt} - V_{wt}$ and $Q_{wt} - \theta_{wt}$ should be avoided. Furthermore, since the magnitude of η_{12} is close to unity, the corresponding input–output pairs (*i.e.*, $P_{wt} - \theta_{wt}$ and $Q_{wt} - V_{wt}$) could be treated as SISO plants. It should be noted that the change of sign at some frequencies in $\eta_{11}(s)$ implies that RHPZs are present in plant $G(s)$, which is consistent with (25). However, it is not clear how those non-minimum phase zeros will affect the control system design and performance arising from the pair definition.

4.3.2. MSF

Using (18) and (21), the MSFs of (25) become

$$\gamma_a = \frac{76.87(s+0.483)(s+0.404)(s^2+0.017s+69.35)(s^2+0.018s+93.34)}{(s+0.535)(s+0.531)(s^2-0.0849s+77.87)(s^2-0.243s+151.9)}$$
$$\gamma_b = \frac{0.013(s+0.535)(s+0.531)(s^2-0.085s+77.87)(s^2-0.24s+151.9)}{(s+0.483)(s+0.404)(s^2+0.0169s+69.35)(s^2+0.0183s+93.34)} \tag{29}$$

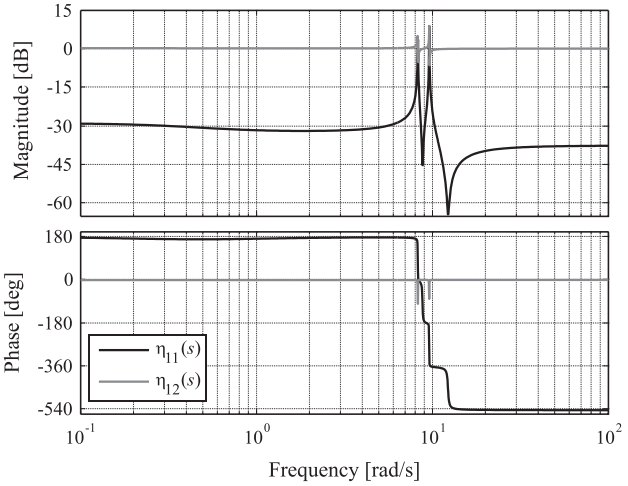

Fig. 5. Bode diagrams of RGA matrix H entries.

An adequate interpretation of the MSFs allows a complete evaluation of the control system design limitations arising from the presence of RHPZs and the multivariable character of the plant. This goes beyond the information provided by the RGA analysis [20]. Since $G(s)$ was obtained from a state-space form, the number of RHPZs of $(1-\gamma_a(s))$ is given by [22]

$$Z = N + P - Q, \tag{30}$$

where Z is the number of RHPZs of $(1-\gamma_a(s))$, P is the number of right hand plane poles (RHPPs) of $\gamma_a(s)$, N is the number of clockwise encirclements to $(1,0)$ in the Nyquist plot of $\gamma_a(s)$, and Q is the number of eigenvalues in the right hand plane of the state-space representation. This is an application of the Nyquist stability criterion [22].

Fig. 6 shows the Bode plots of MSFs $\gamma_a(s)$ and $\gamma_b(s)$. It can be seen that the coupling resulting from pairing $P_{wt}-V_{wt}$ and $Q_{wt}-\theta_{wt}$ is high for all frequencies, as evidenced by the magnitude of $\gamma_a(s)$ above 20 dB. From (29), it is evident that $\gamma_a(s)$ has four RHPPs; *i.e.*, $P=4$. As shown by (25), for this system $Q=0$. Since $\gamma_a(0)=28.85$, the Nyquist plot starts at the right side of $(1,0)$. The Nyquist plot of $\gamma_a(s)$ given in (29) encircles $(1,0)$ four times in counter-clockwise direction, implying that $N=-4$. Thus, applying (30) $(1-\gamma_a(s))$ contains no RHPZs; *i.e.*, $Z=0$.

The information obtained from the previous analysis is revealing. When considering the signal pairs $P_{wt}-V_{wt}$ and $Q_{wt}-\theta_{wt}$, the associated individual channels defined by (17) are non-minimum phase. This is not a consequence of the multivariable character of the plant, as evidenced by the lack of RHPZs in $(1-\gamma_a(s))$, but to those RHPZs appearing in the diagonal transfer functions $g_{11}(s)$ and $g_{22}(s)$ (Eq. (25)). Examination of the Bode plots $g_{ii}(s)$ in Fig. 4 shows that the frequency of those RHPZs is around the frequency of the oscillation mode λ_1. In order to avoid instability, the bandwidth of the oscillation damper should be restricted below the range of frequencies at which it should act to damp electromechanical oscillations. These are two conflicting and irreconcilable control design objectives and, therefore, the MIMO damper design employing signal pairs $P_{wt}-V_{wt}$ and $Q_{wt}-\theta_{wt}$ is not recommended. Even if this was not the case, the fact that $\gamma_a(s)$ has RHPPs implies that $(1-\gamma_a(s))$ will preserve such structure. Thus, the damping controller would require the stabilization of an unstable plant with non-minimum phase zeros, which is not a trivial task [23].

Fig. 6 also shows that the internal coupling of the plant arising from pair $P_{wt}-\theta_{wt}$ and $Q_{wt}-V_{wt}$ is weak: the magnitude of $\gamma_b(s)$ is below -20 dB for most frequencies except for those where the damping controller should act. From (29) it is evident that $\gamma_b(s)$ has no RHPPs ($P=0$). The Nyquist trajectory of $\gamma_b(s)$ given by (29) starts to the left of $(1,0)$ and no encirclements to this point occur, implying that $N=0$. Applying (30), $Z=0$ and thus $(1-\gamma_b(s))$ contains no RHPZs. Moreover, transfer functions $g_{12}(s)$ and $g_{21}(s)$ have no RHPZs. In spite of the presence of RHPZs in $g_{11}(s)$ and $g_{22}(s)$, this does not reflect on the input–output channel definition associated to $\gamma_b(s)$ in (17). Based on this analysis, the input–output pairs $P_{wt}-\theta_{wt}$ and $Q_{wt}-V_{wt}$ should be considered for a MIMO controller design.

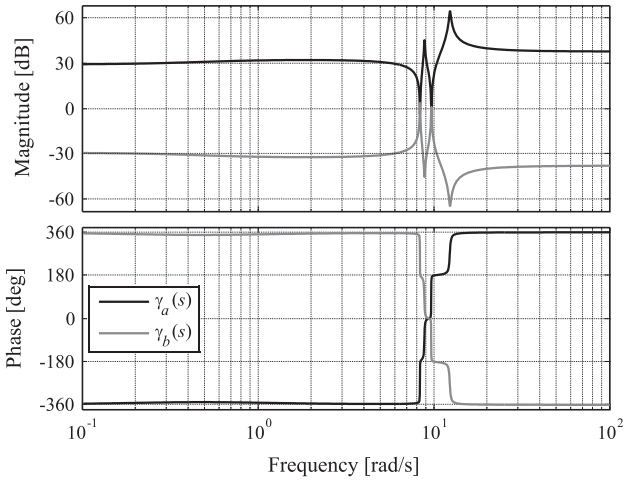

Fig. 6. Assessment of MSFs $\gamma_a(s)$ and $\gamma_b(s)$.

4.4. Simulations

In order to illustrate the previous results, time domain simulations were carried out. The test system of Fig. 3 was implemented in MATLAB/Simulink. A controller of the form $K_{pss}=K(sT_w/(sT_w+1))$ was designed using root locus analysis, where K_{pss} was formed by a washout filter with a time constant $T_w=2$ s, a gain $K=3$ and a limiter. Such a controller structure was used for the case of independent four input–output SISO pairs and when evaluating MIMO configurations. The controller parameters remained the same in all cases to offer a meaningful comparison while ensuring system stability for all SISO cases. In other words, for the following results $K_{pss}=k_{11}=k_{22}=k_{12}=k_{21}$.

Fig. 7 shows the simulation results (input and output variables) for SISO designs considering input–output pairs $P_{wt}-V_{wt}$ and $Q_{wt}-\theta_{wt}$ and for the case of a decentralized MIMO design consid-

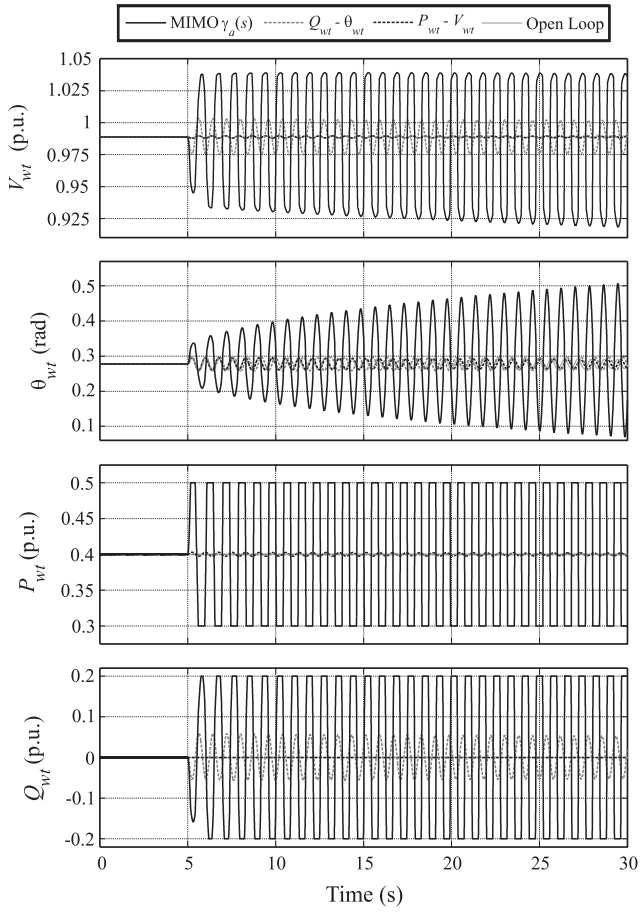

Fig. 7. Simulation responses (voltage magnitude, phase angle of the voltage, active power, and reactive power at WPP bus) for SISO and MIMO designs involving input–output pairs $P_{wt}-V_{wt}$ and $Q_{wt}-\theta_{wt}$.

ering the pairs defined by $\gamma_a(s)$ (*i.e.*, $C_1(s): P_{wt} - V_{wt}$ and $C_2(s): Q_{wt} - \theta_{wt}$). The simulation starts with the system at steady state. At 5s, an impulse variation on the mechanical power reference of the synchronous machine is done in order to excite the oscillation mode existing on the system. As it can be observed, the system becomes unstable for the MIMO design. This was expected since MSF $\gamma_a(s)$ features RHPPs and the simple controllers used are not able to modify its structure. It could be argued that a more complex MIMO controller may stabilize the plant, but this is out of the scope of this work. Conversely, the system is stable when considering the designs for the SISO pairs, but non-minimum phase zeros are present. Moreover, the damping contribution is weak in either SISO case and the oscillations are not damped during the simulation horizon. It could be argued that the performance may be improved by increasing the proportional gain of the controller, but care should be exercised since the system may become unstable due to the presence of RHPZs.

Fig. 8 shows the simulation results for the SISO designs considering input–output pairs $P_{wt} - \theta_{wt}$ and $Q_{wt} - V_{wt}$ and for the case of a decentralized MIMO design considering the pairs defined by $\gamma_b(s)$ (*i.e.*, $C_1(s): P_{wt} - \theta_{wt}$ and $C_2(s): Q_{wt} - V_{wt}$). As it can be seen, in both SISO cases the oscillations are damped after a transient period. When considering the SISO pair $P_{wt} - \theta_{wt}$, the magnitude of the voltage, its phase angle and the reactive power show less oscillations than for the SISO case with $Q_{wt} - V_{wt}$. This was expected from the analysis carried out in previous sections. When using the same controller in both individual channels, it can be seen that the MIMO design produces the best damping performance in all variables except for the case of active power, where the oscillations take a longer time to be eliminated. This superior performance was expected since the MIMO design takes the damping contribution of both feedback loops.

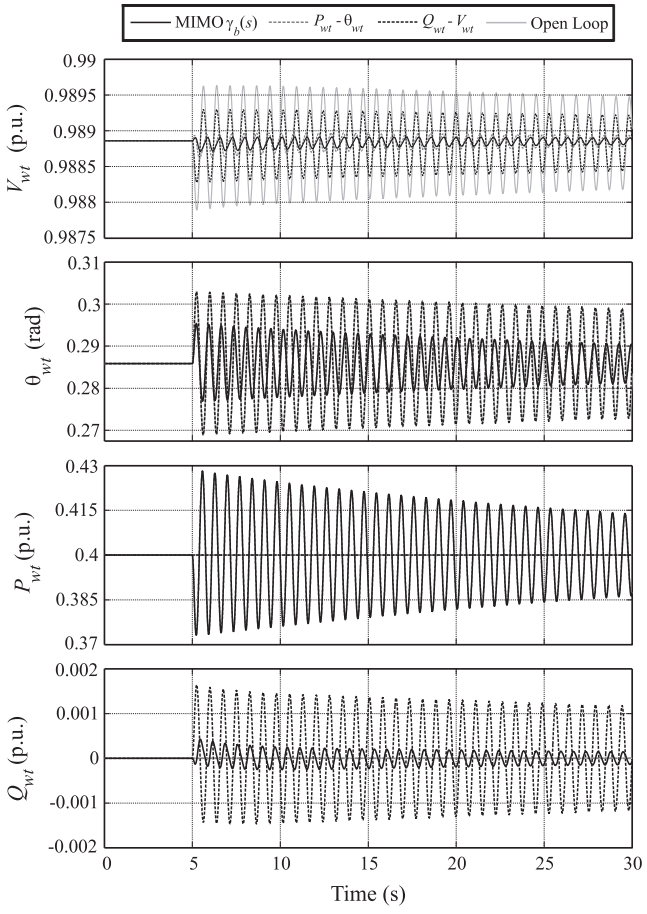

Fig. 8. Simulation responses (voltage magnitude, phase angle of the voltage, active power, and reactive power at WPP bus) for SISO and MIMO designs involving input–output pairs $P_{wt} - \theta_{wt}$ and $Q_{wt} - V_{wt}$.

It should be emphasized that the results obtained in Figs. 7 and 8 agree on well with the analyses carried out with the controllability and observability tools and the frequency domain approaches from the previous sections. It is also apparent that the best performance for any possible SISO alternative is achieved when considering input–output pair $P_{wt} - \theta_{wt}$.

4.5. Recommendations for input–output pair selection

From the analysis of the different selection methods previously presented, some recommendations can be outlined with the aim of finding the most adequate alternative for input–output signal pairing (depending on the desired control scheme).

Considering the SISO case, controllability, observability and the location of RHPZs determine the best signal pair. Various tools for controllability and observability analyses have been presented. The most useful is the geometric measure since erroneous results caused by different magnitude scales are avoided through the normalization of the controllability and observability measures. The location of RHPZs must also be considered in the study since they might impose serious control restrictions if they appear nearby the oscillation mode to be damped.

For decentralized multivariable schemes, the interaction between input–output pairs is also a limiting factor. For this analysis, both RGA and MSF can be used; nevertheless, MSF is more suitable since it provides additional information about the achievable performance levels and limitations associated to RHPZs.

When considering the application of the tools presented in this paper, it is worth noticing that the amount of input and output signals will be reduced when considering WPPs with local signals. This substantially reduces the problem complexity as the system will not present a large system matrix. Following this consideration, it is important to take into account weakly damped oscillation modes only. This helps to further simplify the system when a large number of synchronous generators is present. After these simplifications the tools recommended can be directly applied.

A brief summary of the selection methods discussed in previous sections is given in Tables 5 and 6. The green checkmark indicates the tool capability to provide the marked property, whereas the red cross stands for those properties which cannot be achieved by the selected tool.

Table 5
Controllability and observability tools comparison.

	Cont. and Obs.	Joint O&C	Scale indep.	Control design
PBH	✓	X	X	X
Residues	X	✓	X	✓
Geom. meas.	✓	✓	✓	✓

Table 6
Signal interaction tools comparison.

	Signal coupling	Control design
RGA	✓	X
MSF	✓	✓

Table 7
Power system parameters (in p.u. except indicated) [34].

P_g	P_{wt}	Q_{wt}	E'	ω_s (rad/s)	X_{12}	X_{wt2}	$X_{2\infty}$
0.8	0.4	0	1	100π	0.1	0.1	0.2

Table 8
Synchronous machine parameters (in p.u. except indicated) [34].

T_0	H (s)	X_{ta}	X'
6	4	1.1	0.15 + X_{ta}

Table 9
Operating point, where voltages and angles are in expressed in p.u and in rad, respectively.

E'_0	δ_0	V_{wt0}	θ_{wt0}	V_{20}
1	0.5283	0.9889	0.2858	0.9897
θ_{20}	V_{10}	θ_{10}	V_{ib0}	θ_{ib0}
0.2449	0.9961	0.3262	1	0

5. Conclusion

Several tools have been assessed in this paper to evaluate the potential contribution of WPPs to power system oscillation damping. Efforts have been conducted to choose which of these alternatives is the most adequate. Controllability and observability tests have been analyzed – in particular, those allowing the evaluation of specific oscillation modes (PBH, residues and geometric measures). Among them, the most recommended are the geometric measures since they provide a normalized joint controllability and observability measure. The normalization is useful for the input–output selection because in general the input–output pairs have different scales.

The limitations imposed by the presence of RHPZs on performance have been considered. The stabilization of a plant with RHPZs gives rise to fixed points in the frequency response. As a consequence, if the RHPZs are close to the oscillation modes, there is no controller capable of achieving a substantial increment in damping.

Interactions among input–output pairs were analyzed to assess the possibility of a multivariable control design. RGA and MSF are useful tools to determine the most adequate signal pairs for decentralized control. An advantage of using the MSF analysis over the RGA analysis, in addition to the definition of signal pairs afforded through both approaches, is that the potential dynamic performance and control system design of the oscillation damper can be evaluated. Moreover, through a careful analysis of the MSFs a clear effect of the limitations arising from RHPZs can be clearly defined.

In order to illustrate the different alternatives, a power system including a WPP was analyzed. A simple oscillation damper obtained through classic control design was employed to carry out time domain simulations. Simulation results show a system behavior in agreement with the analyses.

Acknowledgements

The research done by J.L. Domínguez–García, F. Bianchi and O. Gomis-Bellmunt was supported the Ministerio de Economía y Competitividad, Plan Nacional de I+D+i under Project ENE2012-33043, by the EU 7th framework programs FP7-SMARTCITIES-2013 IDE4L Project (under Grant Agreement 608860), by the EU 7th framework programs FP7-ENERGY-2013 IRPWIND Project (under Grant Agreement 609795) and by the European Regional Development Funds (ERDF, "FEDER Programa Competitivitat de Catalunya 2007–2013"). The work carried out by C.E. Ugalde-Loo was supported by the Engineering and Physical Sciences Research Council (EPSRC), Research Councils U.K. (RCUK), under Grant "Centre for Integrated Renewable Energy Generation and Supply (CIRE-GS)," number EP/E036503/1.

Appendix A

The power system, synchronous generator and operating point values are presented as follows (see Tables 7, 8 and 9).

References

[1] Chen Z, Blaabjerg F. Wind farm – a power source in future power systems. Renew Sustain Energy Rev 2009;13:1288–300.
[2] Tsili M, Patsiouras C, Papathanassiou S. Grid code requirements for large wind farms: a review of technical regulations and available wind turbine technologies. In: Proc of the European wind energy conference & exhibition (EWEC'08); 2008.
[3] Domínguez-García JL, Gomis-Bellmunt O, Bianchi F, Sumper A. Power oscillation damping supported by wind power: a review. Renew Sustain Energy Rev 2012;16(7):4994–5006.
[4] Kundur P. Power system stability and control. McGraw-Hill; 1994.
[5] Pipelzadeh Y, Chaudhuri N, Chaudhuri B, Green T. System stability improvement through optimal control allocation in vsc-based hvdc links. IET Gener, Transm Distrib 2012;6(9):811–21.
[6] Díaz-González F, Sumper A, Gomis-Bellmunt O, Villafafila-Robles R. A review of energy storage technologies for wind power applications. Renew Sustain Energy Rev 2012;16(4):2154–71.
[7] Domínguez-García JL, Bianchi F, Gomis-Bellmunt O. Analysis of the damping contribution of power system stabilisers driving wind power plants. Wind Energy 2012 [Early View].
[8] Farsangi M, Song Y, Lee K. Choice of facts device control inputs for damping interarea oscillations. IEEE Trans Power Syst 2004;19(2):1135–43.
[9] Mokhtari M, Khazaei J, Nazarpour D. Sub-synchronous resonance damping via doubly fed induction generator. Int J Electr Power Energy Syst 2013;53:876–83.
[10] De Prada-Gil M, Mancilla-David F, Domínguez-García JL, Muljadi E, Singh M, Gomis-Bellmunt O, et al. Contribution of type-2 wind turbines to sub-synchronous resonance damping. Int J Electr Power Energy Syst 2014;55:714–22.
[11] Domínguez-García JL, Gomis-Bellmunt O, Bianchi F, Sumper A, Sudri-Andreu A. Power system stabiliser capability of offshore wind power plants. In: Proceedings of European wind energy conference & exhibition 2012 (EWEA); 2012.
[12] Hamdan A. An investigation of the significance of singular value decomposition in power system dynamics. Int J Electr Power Energy Syst 1999;21:417–24.
[13] Heniche A, Kamwa I. Assessment of two methods to select wide-area signals for power system damping control. IEEE Trans Power Syst 2008;23(2):572–81.
[14] Zhang Y, Bose A. Design of wide-area damping controllers for interarea oscillations. IEEE Trans Power Syst 2008;23(3):1136–43.
[15] Magaji N, Mustafa M. Optimal location and signal selection of UPFC device for damping oscillation. Int J Electr Power Energy Syst 2011;33(4):1031–42.
[16] Rezaei N, Kalantar M, Shayanfar A, Alipouri Y, Safari A. Optimal IPFC signal selection and damping controller design using a novel current injection model in a multi-machine power system. Int J Electr Power Energy Syst 2013;44(1):461–70.
[17] Li Y, Rehtanz C, Rüberg S, Luo L, Cao Y. Assessment and choice of input signals for multiple HVDC and facts wide-area damping controllers. IEEE Trans Power Syst 2012;27(4):1969–77.
[18] Milanović J, Serrano Duque A. Identification of electromechanical modes and placement of PSSs using relative gain array. IEEE Trans Power Syst 2004;19(1):410–7.
[19] Domínguez-García JL, Bianchi F, Gomis-Bellmunt O. Control signal selection for damping oscillations with wind power plants based on fundamental limitations. IEEE Trans Power Syst 2013;28(4):4274–81.
[20] Licéaga-Castro E, Licéaga-Castro J, Ugalde-Loo CE. Beyond the existence of diagonal controllers: from the relative gain array to the multivariable structure function. In: Proceedings of the 44th IEEE conference on decision and control and 2005 European control conference; 2005. p. 7150–6.
[21] Ugalde-Loo CE, Acha E, Licéaga-Castro E. Fundamental analysis of the electromechanical oscillation damping control loop of the static VAr compensator using individual channel analysis and design. IEEE Trans Power Deliv 2010;25(4):3053–69.
[22] Ugalde-Loo CE. Dynamical modelling of power systems with power electronic controllers using individual channel analysis and design, Ph.D. thesis. University of Glasgow; 2009. <http://theses.gla.ac.uk/1254/>.

[23] Skogestad S, Postlethwaite I. Multivariable feedback control – analysis and design. Chichester (UK): John Wiley & Sons; 2007.
[24] Domínguez-García JL, Gomis-Bellmunt O, Trilla-Romero L, Junyent-Ferré A. Indirect vector control of a squirrel cage induction generator wind turbine. Comput Math Appl 2012;64(2):102–14.
[25] Chen C-T. Linear system theory and design. 3rd ed. New York, NY, USA: Oxford University Press Inc.; 1998.
[26] Ogata K. Modern control engineering. Prentice Hall; 1997.
[27] Pagola F, Pérez-Arriaga I, Verghese G. On sensitivities, residues and participations: applications to oscillatory stability analysis and control. IEEE Trans Power Syst 1989;4(1):278–85.
[28] Heniche A, Kamwa I. Control loops selection to damp inter-area oscillations of electrical networks. IEEE Trans Power Syst 2002;17(2):378–84.
[29] Freudenberg J, Looze D. Right half plane poles and zeros and design tradeoffs in feedback systems. IEEE Trans Automat Contr 1985;30(6):555–65.
[30] Freudenberg J, Hollot C, Middleton R, Toochinda V. Fundamental design limitations of the general control configuration. IEEE Trans Automat Contrl 2003;48(8):1355–70.
[31] Van der Wal M, de Jager B. A review of methods for input/output selection. Automatica 2001;37:487–510.
[32] Leithead W, O'Reilly J. m-input m-output feedback by individual channel design. Part 1. Structural issues. Int J Contr 1992;56(6):1347–97.
[33] O'Reilly J, Leithead W. Multivariable control by 'individual channel design'. Int J Contr 1991;54:1–46.
[34] Elkington K, Knazkins V, Ghandhari M. On the stability of power systems containing doubly fed induction generator-based generation. Electr Power Syst Res 2008;78:1477–84.
[35] Hagstrøm E, Norheim I, Uhlen K. Large-scale wind power integration in Norway and impact on damping in the Nordic grid. Wind Energy 2005;8:375–84.